JOURNAL OF GEOPHYSICAL RESEARCH, VOL. 102, NO. B7, PAGES 15,211–15,224, JULY 10, 1997

Estimating crustal thickness in southern California by stacking PmP arrivals

K. B. Richards-Dinger and P. M. Shearer

Institute of Geophysics and Planetary Physics, Scripps Institution of Oceanography
University of California, San Diego

Abstract. We use observations of the Moho-reflected phase PmP to constrain crustal thicknesses and upper mantle velocities in southern California. We stack normalized absolute values of seismograms from local events in time and range bins after aligning on the initial P arrival and applying a range correction to adjust the various source depths to the surface. Although most individual seismograms do not allow accurate determination of a PmP arrival time, imaging the whole data set in this way shows clear PmP arrivals at ranges from about 90 km to over 250 km. PmP–Pg and PmP–Pn differential times can be measured from the image and used to estimate the Moho depth and upper mantle velocity. For southern California, we obtain an average crustal thickness of 28 km and an upper mantle velocity of 7.8 km/s. Next, we map lateral variations by repeating this procedure for stacks of subsets of the data in which the traces are grouped in caps by Moho reflection point. Estimates of Moho depth range from 18 km in the Salton Trough to 33 km beneath the eastern Transverse Ranges and 36 km beneath the southernmost Sierra Nevada. The upper mantle velocities generally increase from southwest to northeast across the region. We also map postcritical PmP/Pg amplitudes which vary by a factor of 4 with the highest amplitudes in the northwest Mojave Desert. Preliminary experiments with stacking SmS arrivals indicate strongly correlated SmS and PmP amplitude variations. These results provide a guide to source-receiver paths that may produce anomalously strong Moho-reflected phases during future earthquakes.

Introduction

Crustal thickness variations are of fundamental importance to understanding the tectonic evolution and current state of the lithosphere. Owing to the large seismic velocity contrast between the lower crust and upper mantle at the Moho discontinuity, seismology provides the most direct measurements of crustal thickness. Southern California has been particularly well studied, and a variety of seismic methods have been used. These have included both reflection surveys [e.g., *Cheadle et al.*, 1986; *Li et al.*, 1992; *Malin et al.*, 1995] and refraction studies [e.g., *Prodehl*, 1970; *Kanamori and Hadley*, 1975; *Fuis et al.*, 1984], P travel time analyses [e.g., *Hearn*, 1984; *Hearn and Clayton*, 1986; *Magistrale et al.*, 1992; *Sung and Jackson*, 1992; *Zhao and Kanamori*, 1996], and teleseismic receiver function studies [e.g., *Zhu and Kanamori*, 1994; *Baker et al.*, 1996]. Although these results exhibit some differences and have varying coverage and resolution, there is rough agreement that the southern California crustal thickness varies from about 20 to 35 km, with an average value of about 30 km. In general, thinner than average crust seems to occur in the Salton Trough, the far eastern Mojave Desert near the Colorado River, and offshore, whereas thicker than average crust appears to be present beneath the eastern Transverse Ranges (see Figure 1 for the locations of these geographical features). However, the locations of the boundaries between these regions and other details of Moho topography remain somewhat uncertain.

Controlled source reflection and refraction surveys can provide very detailed pictures of crustal structure along linear profiles but are expensive and do not always succeed in penetrating to Moho depths. Teleseismic receiver function analyses often detect Moho-converted phases that constrain crustal thickness (assuming a crustal velocity model) beneath three-component broadband seismic stations. This provides limited coverage since most of the seismic stations in southern California record only short-period vertical ground motion. Pn travel time tomography provides station delays, which are estimates of one-way travel times from the Moho to each station for rays leaving the Moho at the critical angle. Here the coverage in southern California is much better than for receiver functions because all stations can be used. However, it is difficult to separate the

Paper number 97JB00883.
0148-0227/97/97JB-00883$09.00

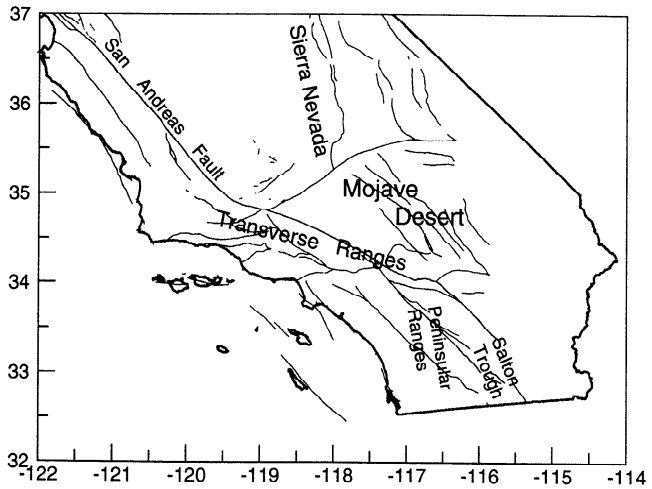

Figure 1. Map of southern California showing the locations of the geographical features mentioned in text.

effects of varying crustal velocities from those of varying crustal thickness. *Sung and Jackson* [1992] address this problem by inverting Pg travel time data for upper crustal velocity variations, which are then taken into account in their Pn study of crustal thickness. However, lower crustal velocity variations remain a potential source of bias.

In principle, the Moho-reflected PmP phase can provide direct constraints on crustal thickness. Unfortunately, PmP arrivals are typically very emergent and are difficult to pick on individual seismograms. Previous studies using data from local earthquakes recorded by the 200+ station Southern California Seismic Network (SCSN) have mainly used travel-time picks of the first-arriving P wave measured by SCSN analysts; such arrival times are not available for PmP. In this paper, we show that clear PmP phases can be imaged by stacking waveforms from hundreds of events. The large number of earthquakes and stations in southern California provides a very good distribution of bouncepoints on the Moho. By grouping records with common Moho bounce points, lateral variations in $PmP-P$ travel times can be measured and used to map crustal thickness and upper mantle velocity. Because PmP and P have similar ray parameters, their differential time is little affected by event mislocations and near-station and upper crustal velocity variations. However, velocity variations in the lower crust are still a source of ambiguity.

Using this waveform stacking approach, we produce

neath southern California. In addition, we find systematic differences in PmP and SmS amplitudes that may be related to shorter-wavelength Moho topography.

Data and Processing

Data

Our data are digital waveforms recorded by the U. S. Geological Survey (USGS)/Caltech Southern California Seismic Network (SCSN) [*Wald et al.*, 1995] of more than 200 stations (see Figure 2b). While some of these are multicomponent stations, we use only the short-period, vertical-component seismographs that make up the bulk of the network. Data from the stations are telemetered into Pasadena and then digitized at sample rates that have varied between 50, 62.5, and 100 Hz.

Records from over 220,000 local events are available from 1981 to 1994. To achieve as even a distribution of sources as possible, we selected 4,625 of these events using the following criteria. We use only events with "A" quality locations (<1 km horizontal and <2 km estimated vertical standard errors). We then divide the catalog into bins 0.08° by 0.08° by 5 km by 0.5 units in latitude, longitude, depth, and local magnitude, respectively, with depths down to 20 km and magnitudes from 2.0 to 4.0. We do not use any events larger than M=4 since waveforms from the larger events are usually clipped. From each bin that contains an event, we select the event with the largest magnitude (see Figure 2a). Each of these events was recorded by an average of 79 stations within our epicentral distance range of interest (0 km to 250 km), for a total of 366,822 seismograms.

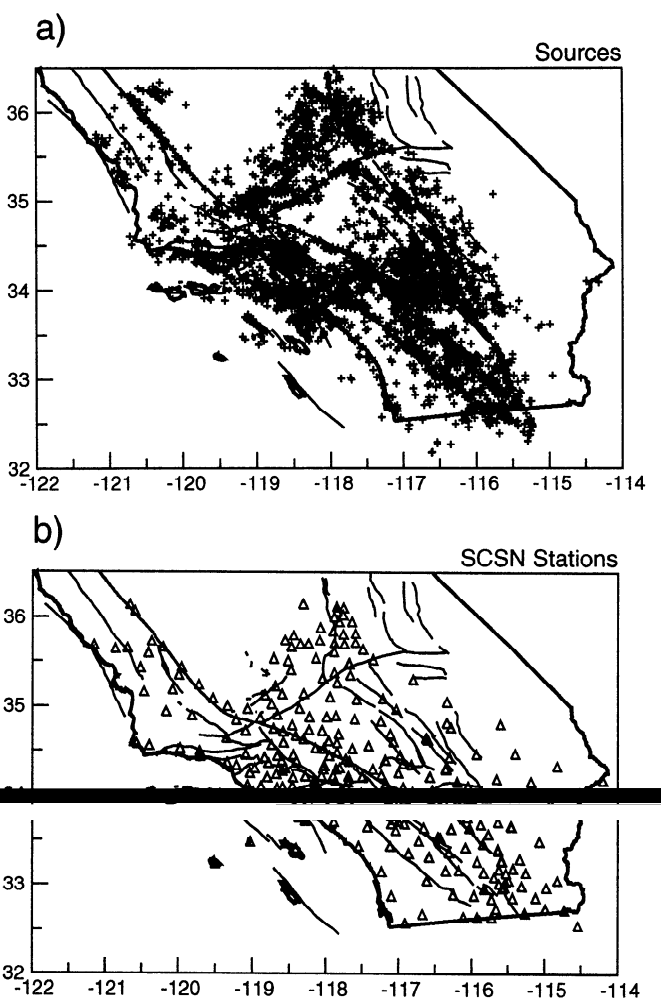

Figure 2. (a) Locations of sources used in this study. Heavy lines are state boundaries and coastlines; light lines are faults. (b) Locations of SCSN stations used in this study.

Stacking Procedure

Since on most of these seismograms it is difficult to identify PmP, much less pick its arrival time, we process and stack the records as follows:

1. We low-pass filter the seismograms with a cutoff frequency of 10 Hz. This improves the signal-to-noise ratio somewhat over the raw seismograms. We also resample the records to a uniform sample rate of 100 Hz.

2. Since only some of the seismograms had P arrival times picked by analysts, we run the autopicker of *Earle and Shearer* [1994] on each record. This autopicker returns several pick times for each seismogram, along with a short-term average to long-term average (STA/LTA) ratio for each pick. We select as the P wave arrival the pick with the largest STA/LTA of those that are within 0.75 s of the first arrival time predicted using a standard one-dimensional (1-D) southern California seismic velocity model [*Hadley and Kanamori*, 1977; *Wald et al.*, 1995] (hereafter referred to as the HK model, this model consists of three homogeneous crustal layers over a homogeneous half-space: a 5.5 km thick upper crustal layer at 5.5 km/s, a 10.5 km thick midcrustal layer at 6.3 km/s, a 16 km thick lower crustal layer at 6.7 km/s, and a mantle half-space at 7.8 km/s). If no such picks exist, we discard the seismogram. This reduces the number of records to 201,284.

3. We form a P signal-to-noise ratio by dividing the root-mean-square value of the seismogram in a 0.5 s window following the P arrival time by that for a similar window ending 1.0 s before the P arrival time. If this ratio is less than 3.0, we discard the record. This leaves us with 145,151 seismograms.

4. We normalize each seismogram to its peak P wave amplitude by dividing by the largest value between 0.2 s before and 0.5 s after the P arrival time. Since only relative amplitude information is used, the effects of differing source magnitudes, radiation patterns, source-receiver ranges, and local site amplifications are greatly reduced.

5. We align on the first-arriving P wave as a reference phase by adjusting the start time of each seismogram to be zero at the P arrival time.

6. Because of the large variations in source mechanisms, local site responses, etc., we do not expect the waveforms to be similar enough that individual wiggles will stack coherently. However, we do hope to have energy from the PmP phase arriving at similar delays from P on the different records. Therefore we take the absolute value of the traces prior to stacking (we have found that this gives results that are virtually indistinguishable from using the envelope function [e.g., *Kanasewich*, 1973] but at less computational cost).

7. For seismograms with the same source-receiver range, the delay times between PmP and P will vary with source depth. Therefore we assign a "corrected" source-receiver range to each record such that the predicted (using the HK model) PmP–P time for the actual source depth and source-receiver range is equal to the predicted PmP–P time for a surface source at the adjusted range.

8. Finally, we average the processed seismograms in time and range bins (0.05 s by 3 km) to produce images of the wavefield.

Figure 3 shows typical Pg, Pn, and PmP ray paths and their associated travel time curves. Note that all three ray types have similar paths near the receiver. Since we are concerned only with relative arrival times, this allows us to neglect corrections for station elevation and for station delays due to near-receiver velocity variations. However, the correction for source depth is significant since we use sources as deep as 20 km (for comparison, most station elevations are within 1 km of sea level and all are within 2.5 km). Figure 3c shows the result of aligning on the first-arriving P wave. Since

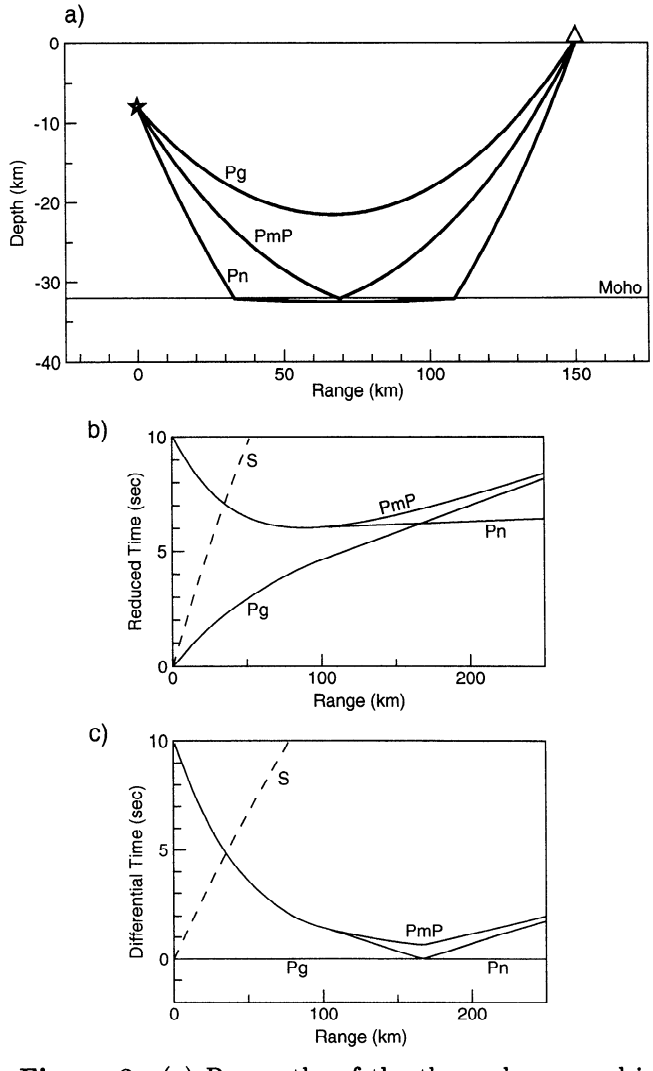

Figure 3. (a) Ray paths of the three phases used in this study, for a source depth of 8 km and an epicentral range of 150 km. (b) Travel time curves for the three phases and S, for a surface source, reduced at 8 km/s. Calculation assumes a smoothed version of the standard Hadley-Kanamori velocity model. (c) The same travel time curves aligned on the first arriving P wave, i.e., Pg at ranges less than the Pg/Pn crossover range and Pn at further ranges.

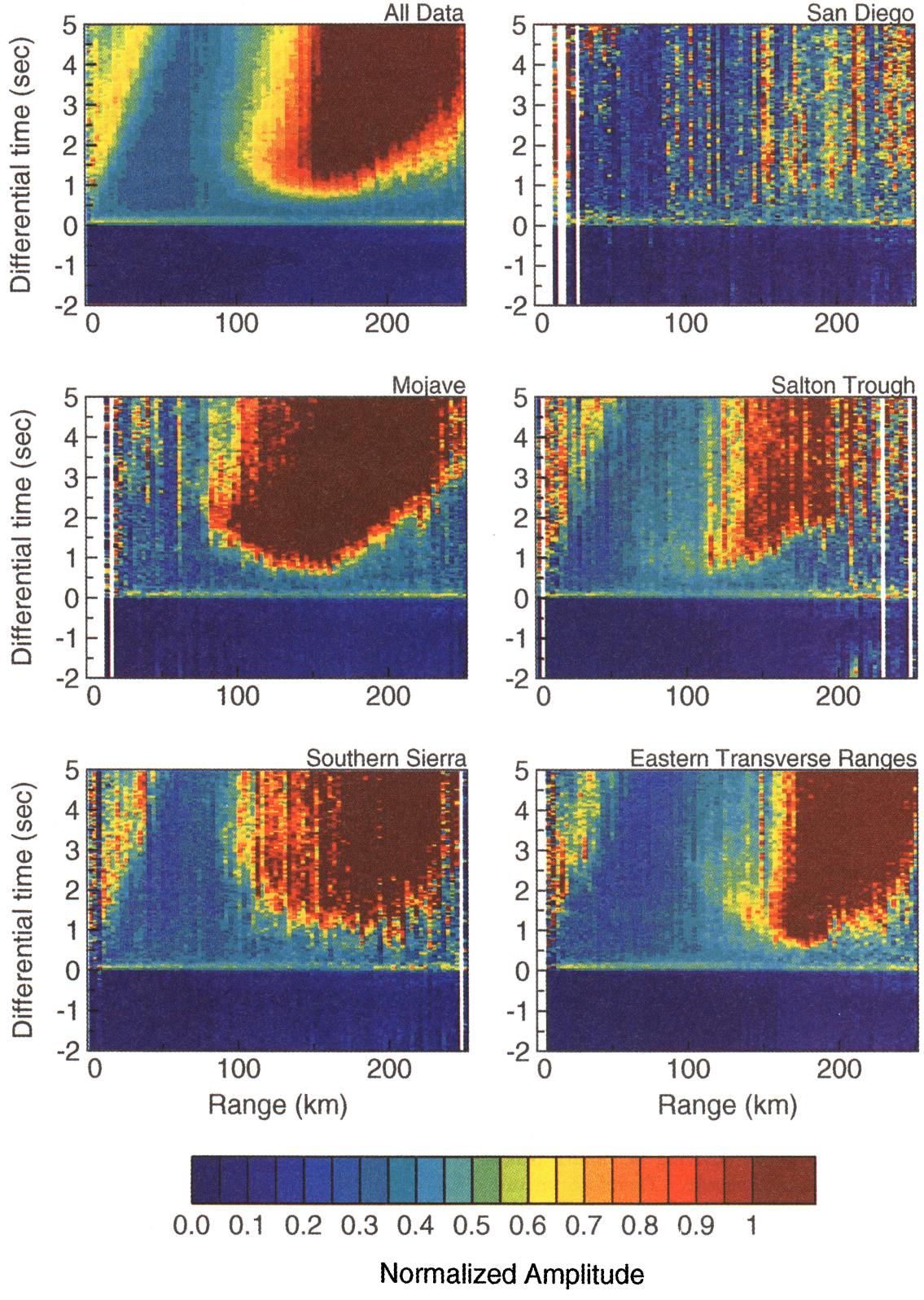

Plate 1. Time versus range images of stacked waveforms for the entire data set (top left) and of stacks for individual bounce point caps. Plots are labeled with the approximate location of the cap. The first-arriving P waves are aligned at zero time; PmP is seen arriving 1 to 2 s later at ranges beyond about 100 km.

this arrival switches between Pg and Pn at the Moho crossover point, this introduces kinks in the Pg, Pn, and PmP travel time curves at the crossover range.

The top left plot of Plate 1 shows the result of applying this procedure to our entire data set. The P arrival is quite sharp, rising from the noise level to peak values of 0.5 to 0.6 within 0.1 s. The maximum P values in the stack are not 1.0, because while we normalize each seismogram to have unit peak P amplitude, we align not on the time of the peak but on the autopick time. Because of waveform variations, the peak values occur at differing delay times from the arrival times. S is visible at small ranges before disappearing off the top of the plot. Comparison of the stacked image with the theoretical travel time curves in Figure 3c shows that the moveout (relative to P) of the high-amplitude phase arriving 0.75 s to 2.5 s after P between ranges of 90 km and 250 km agrees reasonably well with that predicted for PmP by the HK velocity model. Even better agreement can be achieved by retaining the HK crustal velocities but moving the Moho from 32 km to 28 km.

To investigate lateral variations of PmP within southern California, we repeat the stacking procedure using subsets of the data. Specifically, we consider a grid of points which covers southern California with a spacing of 0.25° in both latitude and longitude and form a stack for each grid point using only those seismograms whose Moho bounce points (calculated assuming the HK velocity model) are within 25 km of the grid point (we will refer to these regions surrounding each grid point as bounce point caps). This is similar in some respects to common midpoint stacking methods in reflection seismology; however, our analysis is complicated by the fact

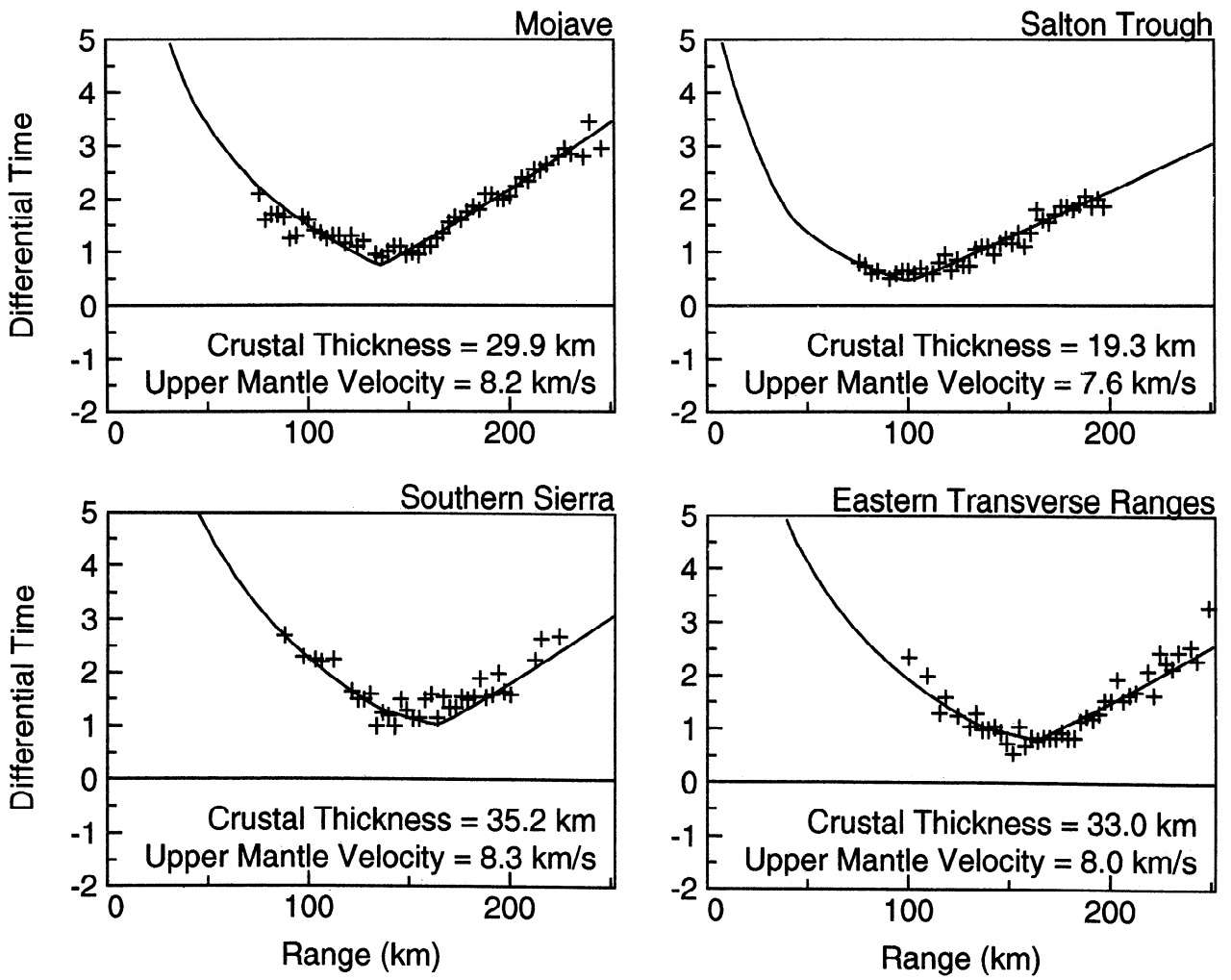

Figure 4. Each of these four plots corresponds to each of the bounce point cap stacks in Plate 1 for which a clear PmP arrival can be identified. The crosses are the $PmP - P$ differential times picked (automatically) from the stacked traces. The theoretical $PmP - P$ curve which best fits (in the sense of minimizing the 1-norm of the misfit) these times is shown. The crustal thickness and upper mantle velocity which achieve this minimum misfit are indicated in the lower part of each plot.

that we cannot simply use the source-receiver midpoint due to the large variations in source depth. Five examples of these grid point stacks are shown in Plate 1.

In the majority of these localized stacks, a PmP arrival is clearly visible. Most of the exceptions are for grid points near or beyond the edge of the network where the data are sparse. The image for a grid point to the northeast of San Diego (top right plot in Plate 1) is an unusual example of a stack containing considerable data that shows no clear PmP arrival. The other four bounce point caps plotted in Plate 1 display clear PmP arrivals. Note that the PmP arrival in these localized stacks is more impulsive than that in the stack of the entire data set. Presumably, this reflects the fact that the crust in the local regions around each grid point is more constant in depth than the crust in southern California as a whole.

The amplitude of the PmP arrival in the stacks is quite variable, with the Mojave grid point stack having the highest and the Salton Trough the lowest amplitudes of the four examples shown. The timing of the PmP arrival also varies with respect to Pg and Pn. It is particularly easy to see the different ranges at which the PmP–P differential time is minimized. This is the Pg/Pn crossover range. In the four examples shown, this crossover range varies from 100 km for the Salton Trough grid point to 170 km for the southern Sierra grid point. We use these variations in timing to estimate the crustal thickness and upper mantle velocity variations in southern California as described below.

Picking and Fitting Procedure

The stacked traces with visible PmP arrivals generally consist of (1) low amplitudes (<0.1) before the P arrival, (2) a rise to a peak P value of ~0.5 within 0.1 s of the first break in the P wave, (3) a drop to about 0.3 to 0.4, and (4) a (sometimes gradual) rise to peak PmP values of up to 3.0. Since the PmP arrival often has a gradual onset, it is not always clear where to pick the arrival time. We select the time when the stacked trace first exceeds a threshold value set halfway between the local minimum value following the P pick and the peak PmP value. We do not pick PmP times at ranges less than 75 km to avoid misidentifying the S arrival as PmP.

We also calculate several proxies for PmP signal-to-noise ratios and discard picks from traces for which these proxies fall below a threshold. For each Moho bounce point cap, we obtain a set of PmP–P differential travel times at several different ranges. Next, we fix the velocities in the crust at the HK model velocities but perform a grid search over Moho depth and upper mantle velocity to find the values of these parameters which minimize the 1-norm of the misfit between the predicted and observed PmP–P differential travel times.

In Figure 4 we show the results of applying this procedure to the four grid point stacks from Plate 1 that have clear PmP arrivals. In general, the theoretical curves

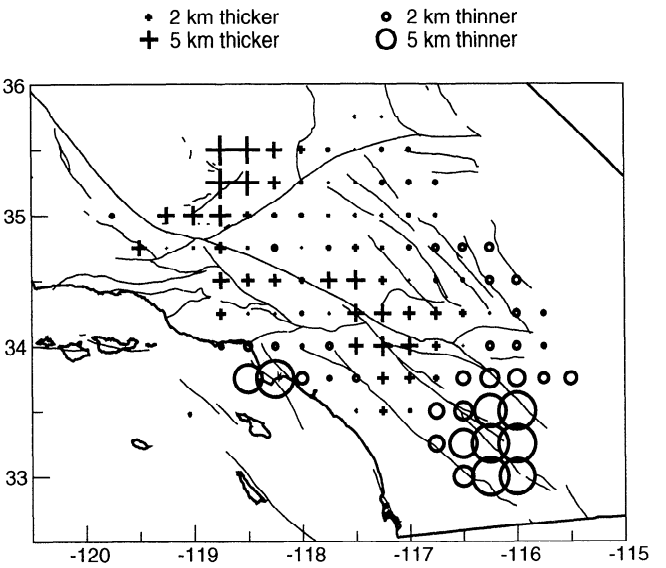

Figure 5. Our estimates of crustal thickness for each Moho bounce point cap which has a clear PmP arrival. The thicknesses are plotted relative to an average of 28.2 km.

fit the observed arrival times well; in the four examples shown, the average misfit ranges from 0.09 s for the Salton Trough grid point stack to 0.20 s for the southern Sierra stack. Note the variations in the inferred crustal thicknesses, which range from 18 to 36 km, and the upper mantle velocities, which vary from 7.6 to 8.3 km/s. The crustal thickness is mainly constrained by the crossover point (indicated by the minimum PmP–P time), while the upper mantle velocity is constrained mostly by the slope in the PmP arrivals at ranges beyond the crossover. A fixed lower crustal velocity of 6.7 km/s is used in the fitting procedure; there is some trade-off between this assumed velocity and our inferred crustal thicknesses and upper mantle velocities (see next section).

In Figure 5 we plot the crustal thickness estimates from all the grid point stacks containing valid PmP arrival times from at least 15 different range bins and for which the average misfit between these observed PmP–P times and those predicted by the best fitting crustal thickness and upper mantle velocity is 0.25 s or less. These crustal thicknesses should be regarded as averages over circular areas with diameters of 50 km. The pattern of crustal thickness variation is spatially quite coherent. Some coherence might be expected between adjacent bins, since they have about 50% of their data in common (assuming a uniform distribution within each cap). However, the scale length of the observed variations spans several grid points, including bins with no common data, suggesting that this coherence is a real feature of the data.

Plate 2 shows a contour map of the crustal thickness estimates from Figure 5, together with our results for upper mantle velocities. Blue indicates thicker crust

in the top plot and faster *Pn* velocities in the bottom plot, while red denotes thinner crust and slower velocities. Note that thinner crust is indicated near the Salton Trough and offshore, while there appears to be thicker crust beneath the eastern Transverse Ranges and the southern Sierra. The upper mantle velocities are slower to the southwest and faster to the northeast. Before discussing the implications of these results, let us first examine the assumptions of our modeling method in more detail.

Limitations and Probable Error Bounds

Our stacking and modeling procedure should produce unbiased results only under certain idealized conditions. These include the following: (1) the crustal velocity structure is one-dimensional and, moreover, is equal to the HK model; (2) the Moho is a horizontal plane with zero dip; (3) the catalog locations of the events are correct; (4) the upper mantle is isotropic; and (5) the two automatic picking algorithms are correctly picking the *P* time from the individual seismograms and the *PmP* times from the stacked traces.

To evaluate the importance of several of these assumptions, we perform tests in which we generate synthetic *PmP–P* times from models that deviate from our idealized model by the maximum expected amount. We then apply our grid search procedure to see how much our estimates of crustal thickness and upper mantle velocity are biased from their true model values. To test the effect of variations in crustal velocity, we change each layer of the HK model by the largest expected deviation for southern California. For instance, since the uppermost layer of the HK model is appropriate for stations at hard rock sites, we take as an extreme perturbation to the first layer in the HK model an example from a basin filled with several kilometers of sediment. *Fuis et al.* [1984] found near-surface velocities of 2 km/s increasing to 5.5 km/s at 5 km depth in the central part of the Salton Trough. Using this model, we find that our estimated crustal thickness is 1.3 km too thin and our estimated upper mantle velocity 0.01 km/s too slow. Thus, even a rather large change to the upper crustal velocities has virtually no effect on the inferred upper mantle velocity and only a small impact on the Moho depth; as noted earlier, this is due to the relative insensitivity of *PmP–P* differential times to upper crustal velocity variations.

Velocity perturbations in the middle and lower crust are expected to be much smaller than those in the upper crust. *P* travel time tomography studies with resolution widths similar to our study find a maximum of ±3% variations in crustal velocities [e.g., *Sung and Jackson,* 1992]. A velocity increase of 3% in the 10.5 km thick midcrustal layer results in crustal thickness estimates that are 1.6 km too thick and upper mantle velocities that are 0.02 km/s too fast. For the 16 km thick lower crustal layer, a velocity increase of 3% causes our estimate of Moho depth to be 1.5 km too shallow and inferred upper mantle velocity to be 0.27 km/s too slow. Changing the sign of the perturbation also changes the sign of the biases. Typical errors should be less than these values since not only are these extreme perturbations to our assumed model, but also in each local bounce point stack, we are using stations and receivers at many different ranges and azimuths, which should serve to average out the biases.

Note that the upper mantle velocity estimates are significantly affected only by variations in the lower crustal velocity; there is a direct trade-off between upper mantle and lower crustal velocities. This is due to the fact that the slope of the *PmP–P* times beyond the *Pn* crossover range is controlled almost completely by the slowness difference between the lower crust and upper mantle. In the last example, the synthetic times were generated from a model with lower crustal and upper mantle velocities of 6.9 and 7.8 km/s, respectively, for a slowness contrast of 0.0167 s/km. In our grid search procedure, we assumed a lower crustal velocity of 6.7 km/s; therefore our estimated upper mantle velocity was biased downward to 7.53 km/s, such that the slowness contrast stayed nearly constant (0.0165 s/km difference between the assumed lower crustal and estimated upper mantle slownesses). We can determine the slowness contrast across the Moho significantly better (by a factor of 3) than we can constrain the upper mantle or lower crustal velocities separately.

Even if the crustal velocity profile is equal to our assumed model, a dipping Moho could bias our estimates of crustal thickness and upper mantle velocity. Our stacking procedure minimizes this effect by combining data with common bounce points, but does not eliminate it completely. The steepest large-scale Moho dips present in our map are about 10°. Simple synthetic tests show that such slopes, if shooting along dip, bias our estimate of Moho depth to values that are 2 km too shallow and our estimate of upper mantle velocity about 0.11 km/s too slow. If shooting along strike, our estimate of Moho depth is biased 0.5 km too shallow, and our estimate of upper mantle velocity is not affected. Good azimuthal coverage should lead to biases at intermediate values. In any case, the errors introduced by neglecting the Moho dip are small compared to the size of the Moho topography that we observe.

In an attempt to reduce biases due to source mislocations, we use only events for which the SCSN catalog lists an A location quality. These are events for which the estimated horizontal and vertical standard errors are less than 1 km and 2 km, respectively. Horizontal mislocation errors have a negligible effect on our estimates. A 2 km error in source depth will bias our estimate of crustal thickness approximately 0.5 km in the opposite direction and have virtually no effect on the upper mantle velocity. However, if the vertical source location errors are distributed symmetrically about zero, these biases should also average to zero,

since each local crustal thickness estimate uses data from many different sources.

Previous studies have found evidence for upper mantle azimuthal anisotropy of up to 5% in southern California [*Vetter and Minster,* 1981; *Hearn,* 1984; *Sung and Jackson,* 1992; *Hearn,* 1996]. In this study we have not allowed for the effects of Pn anisotropy. If the seismograms in each bounce point stack are uniformly distributed in azimuth, then any anisotropic contribution to the upper mantle velocity should be averaged out. In the bottom plot of Figure 6 we show the azimuth distribution of seismograms at Pn ranges for each bounce point stack. Most of the bounce point stacks have decidedly nonuniform azimuth distributions, with some being very dominated by quite narrow azimuth ranges. For this reason, inverting for anisotropic parameters would be difficult since there is a trade-off between the anisotropy and lateral velocity variations. Our estimates should be considered a reliable measure of the azimuthally averaged velocity only for those bounce points with suitable ray coverage. For the bounce points with limited coverage, the upper mantle velocity we determine should be interpreted as the velocity for rays traveling at the dominant azimuth. Fortunately, our Moho depth estimates are not affected by Pn anisotropy.

There is some uncertainty about the origin of the large-amplitude secondary arrival seen in our stacks. Its relative arrival time as a function of range agrees with that of PmP, and we are interpreting it as such, but other secondary phases may be present, including Pn (when Pg is the first arrival), Pg (when Pn is the first arrival), and free-surface reflected and converted phases. Synthetic seismogram modeling (or even simple geometrical spreading considerations) gives very small amplitudes for Pn (much smaller than either Pg or PmP), so it is not surprising that it does not appear as a secondary arrival in our stacks; it is unlikely to interfere with measurement of the PmP–P differential travel times at ranges less than the Pg/Pn crossover range. Most of the free-surface reflected and converted phases either have small amplitudes and/or arrive well after PmP. The only possible exception is sP, which for shallow ($< \sim$5 km) sources can have a substantial amplitude and arrive before PmP for ranges less than $\sim$100 km. However, since the arrival time of sP (as for all depth phases) is very sensitive to source depth, our stacking procedure should greatly reduce its amplitude. Also, sP has a very different moveout from PmP and so should be easily distinguishable (by eye) from PmP. None of the stacks from which we are estimating a crustal thickness show signs of sP.

The question of Pg as a secondary arrival at ranges beyond the Pg/Pn crossover is more troublesome. The $Pg - P$ travel time is not as sensitive to source depth as the depth phases discussed above; the stacking procedure will not eliminate Pg nearly as well as it does the depth phases. However, Pg is not seen as a distinct secondary phase in our data stacks. In stacks of synthetic seismograms made for a range of source depths, Pg is visible between Pn and PmP at distances beyond the crossover (though the Pg amplitude is sensitive to the assumed lower crustal velocity gradient and the stacking procedure does reduce its amplitude somewhat from that for sources at a single depth). When our picking procedure is run on such stacks, it does indeed pick Pg instead of PmP for ranges more than 10 km beyond the Pg/Pn crossover range. Fitting these picks results in underestimates of 0.7 km in the crustal thickness and 0.2 km/s in the upper mantle velocity. An additional check on how much Pg contamination might be affecting the crustal thickness estimates is provided by rerunning our fitting procedure on the data using only those picks from range bins less than 125 km (originally we used ranges out to 250 km). Since Pg contamination is a possible problem only for ranges more than $\sim$10 km beyond the Pg/Pn crossover range, these estimates should be much less affected by any possible Pg contamination. The resulting crustal thickness estimates agree well with the original ones, with > 80% of

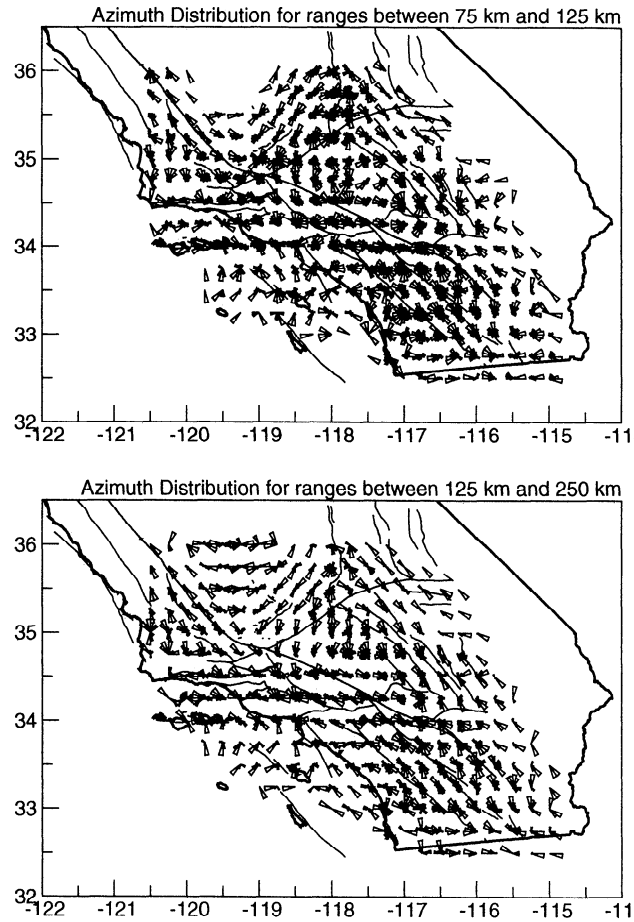

Figure 6. Azimuth distributions of the seismograms which are stacked in each Moho bounce point cap. (top) The azimuth distributions for seismograms with ranges for which the first arrival is usually Pg, and (bottom) the distributions for ranges for which the first arrival is usually Pn.

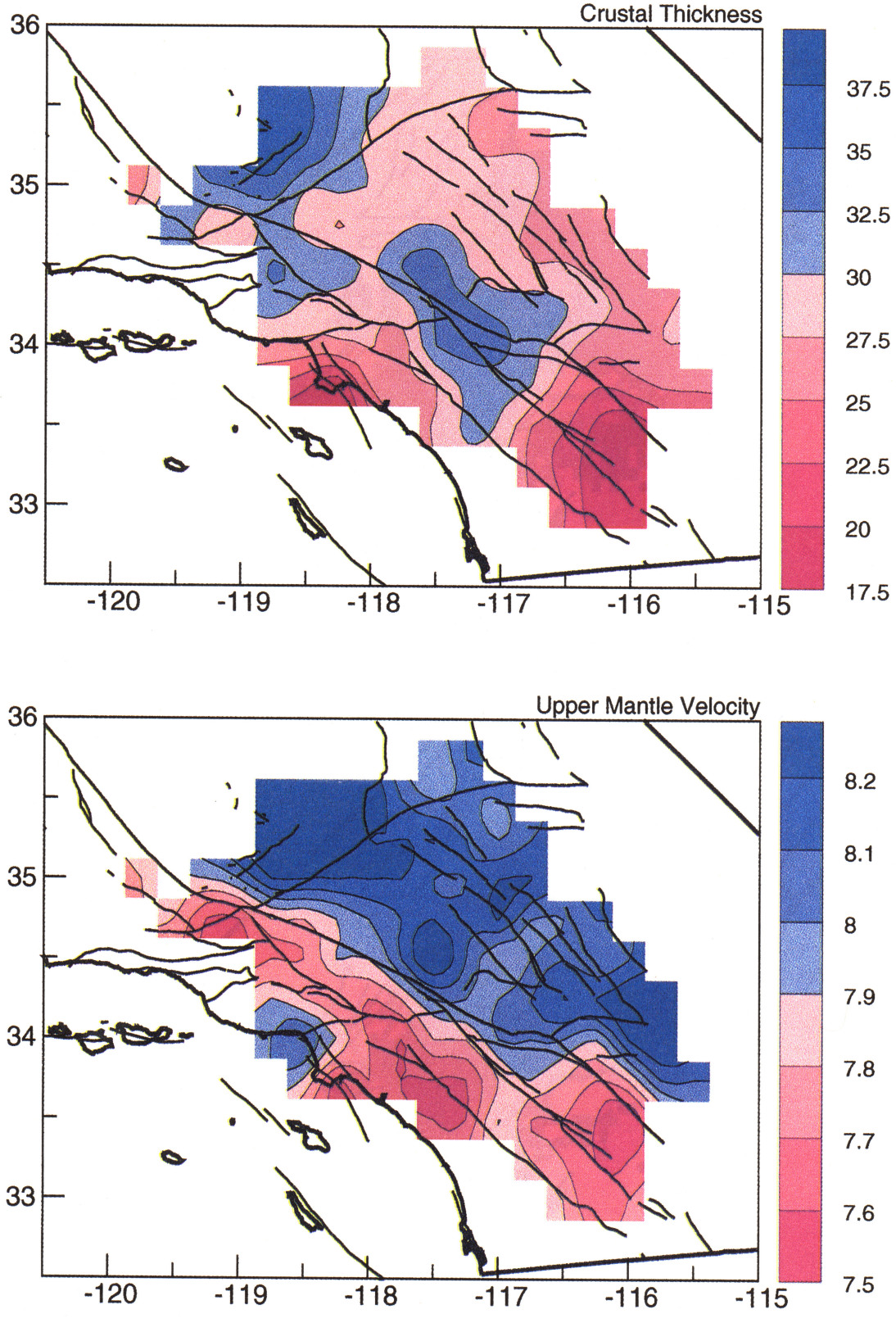

Plate 2. Contour plots of (top) our crustal thickness estimates and (bottom) upper mantle velocity estimates. Crustal thicknesses are in kilometers and upper mantle velocities are in kilometers per second. Results are relative to an assumed lower crustal velocity of 6.7 km/s; variations in lower crustal velocity will have a relatively small effect on crustal thickness but will significantly bias the upper mantle velocities.

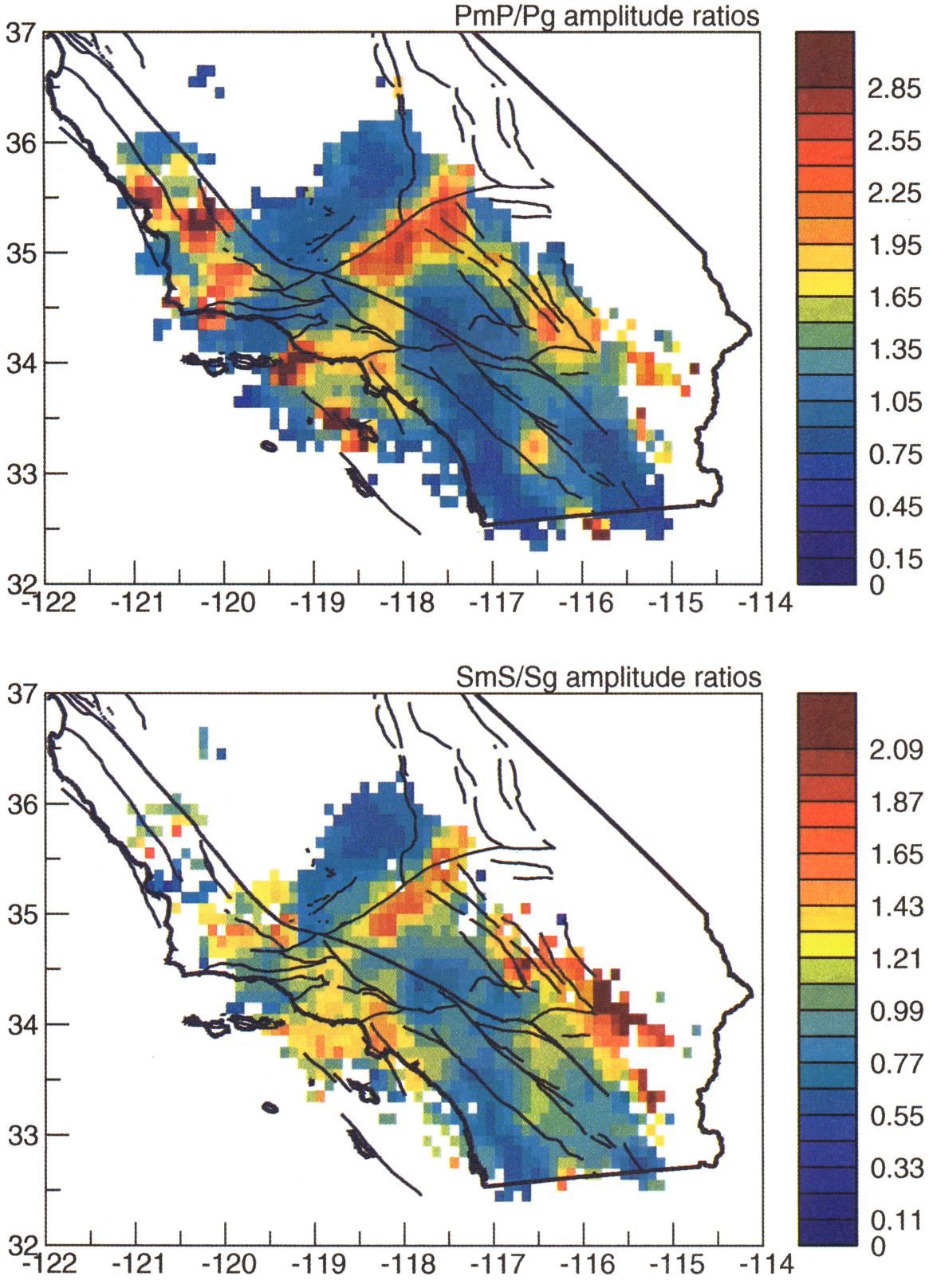

Plate 3. (top) PmP/Pg amplitude ratios and (bottom) SmS/Sg amplitude ratios. The SmS/Sg amplitude variations are well correlated with the PmP/Pg variations but are slightly weaker (note the change in scale between the plots).

the estimates within 0.5 km and > 90% within 1.0 km. In summary, it is not clear whether or not Pg contamination beyond the crossover range is a problem, but our crustal thickness estimates seem to be reasonably robust with respect to this possibility.

Finally, there is some level of uncertainty associated with the scatter in the measured P and PmP travel times and the fitting procedure for each 50 km diameter bounce point cap. Based on how the misfit varies away from the minimum in parameter space, we estimate uncertainties of ±1.0–1.5 km in crustal thickness and ± 0.1–0.15 km/s in upper mantle velocity, assuming a fixed lower crustal velocity. The spatial coherence of our results (see Plate 2), even between bounce point caps that share no data, also limits the size of any random errors involved in our method.

Of all the sources of bias considered here, lower crustal velocity variations are the most important. Our inferred Moho depths and upper mantle velocities are relative to the assumed lower crustal velocity model. Ultimately, it would be advantageous to combine our PmP results with P travel time tomography estimates of lower crustal velocities.

PmP and SmS Amplitudes

As mentioned earlier, the bounce point stacks show that the amplitude of the PmP arrival varies within southern California. In the top plot of Plate 3 we show a map of average PmP/Pg amplitude ratios at source-receiver ranges between 60 and 110 km. To make this image, we form a PmP/Pg amplitude ratio for each seismogram by taking the ratio of the rms values of the seismogram in two 0.5 s windows. The Pg window begins at the time of the autopicked Pg time and the PmP window is delayed from that by the theoretical PmP–Pg differential time calculated from the HK crustal model. We then group these individual ratios by Moho bouncepoint in 0.1° latitude by 0.1° longitude bins and take the average within each bin. Finally, we smooth the resulting image by applying a nine point median filter to each bin. Note that for areas with crust thinner than ~22 km the Pg/Pn crossover range is less than 110 km. So for those areas (i.e., the Salton Trough and offshore), there are some PmP/Pn ratios averaged in with the PmP/Pg ratios which will therefore overestimate the average PmP/Pg ratio in those areas.

The amplitudes shown in Plate 3 (top) exhibit smooth spatial variations, with areas of high average PmP amplitude in the Mojave (especially in the northwest), extending south to offshore of Los Angeles, and a region extending from Santa Barbara to San Luis Obispo. Areas of low PmP amplitudes are found in the southern Sierra Nevada and in a large region extending from the southern Mojave southeast into the Salton Trough as well as south through the eastern Transverse Ranges and the Peninsular Ranges to San Diego. To test the robustness of this result, we have produced analogous images using seismograms restricted to particular azimuth and distance ranges. While there are some differences, these images are all similar to the result for the entire data set. This stability suggests that the amplitude variations are due to structure near the Moho bounce points, rather than focal mechanism differences, near-source or near-receiver structure, or uneven sampling of range dependence in the PmP amplitudes.

However, there is also the fundamental ambiguity that variations in either PmP or Pg could be causing the variations in the PmP/Pg amplitude ratio. Some measure of absolute amplitudes is provided by the ratio of our observed amplitudes to the noise levels before the P arrival. In the waveform stacks, the P amplitude-to-noise ratios are fairly constant, while the PmP-to-noise ratios vary widely. This suggests that the bulk of the PmP/P amplitude variations are caused by changes in the PmP amplitude.

To compare with our PmP results, we have performed a preliminary investigation of SmS arrivals for 961 of the 4625 events that we analyzed for PmP. These events yield 88,081 seismograms, which we process to determine SmS/Sg amplitude ratios using the same technique previously described for PmP/Pg. The SmS/Sg amplitude variations are shown in Plate 3 (bottom); note the high correlation of this pattern with the PmP/Pg amplitudes, suggesting a common origin for both. SmS amplitudes are important not only for information they may provide about the Moho but also because it has been suggested that at certain epicentral distances, the strongest ground motions following some large earthquakes have been produced by postcritical S reflections from the Moho [e.g., *Somerville and Yoshimura,* 1990; *Mori and Helmberger,* 1996]. Thus these maps could be used in seismic hazard assessment to identify source-receiver paths that might be expected to produce anomalously large amplitudes at ranges beyond about 60 km.

Since these amplitude variations can be seen at postcritical ranges, they cannot arise from differences in the Moho reflection coefficient. Possible causes include focusing and defocusing of PmP due to long-wavelength topography on the Moho and/or lateral variations in lower crustal velocities, variations in the degree of scattering at the Moho due to short-wavelength Moho topography or crustal heterogeneities near the Moho, and differences in intrinsic attenuation. Investigating the causes of these amplitude variations will be the subject of future work.

Discussion

The main features of the map of our crustal thickness estimates are (1) a nearly flat Moho at about 30 km in the Mojave Desert, thinning slightly to the east, (2) very thin (< 20 km) crust in the Salton Trough, (3) thicker than average crust (up to 33 km) under the eastern Transverse Ranges, (4) thin crust offshore of the

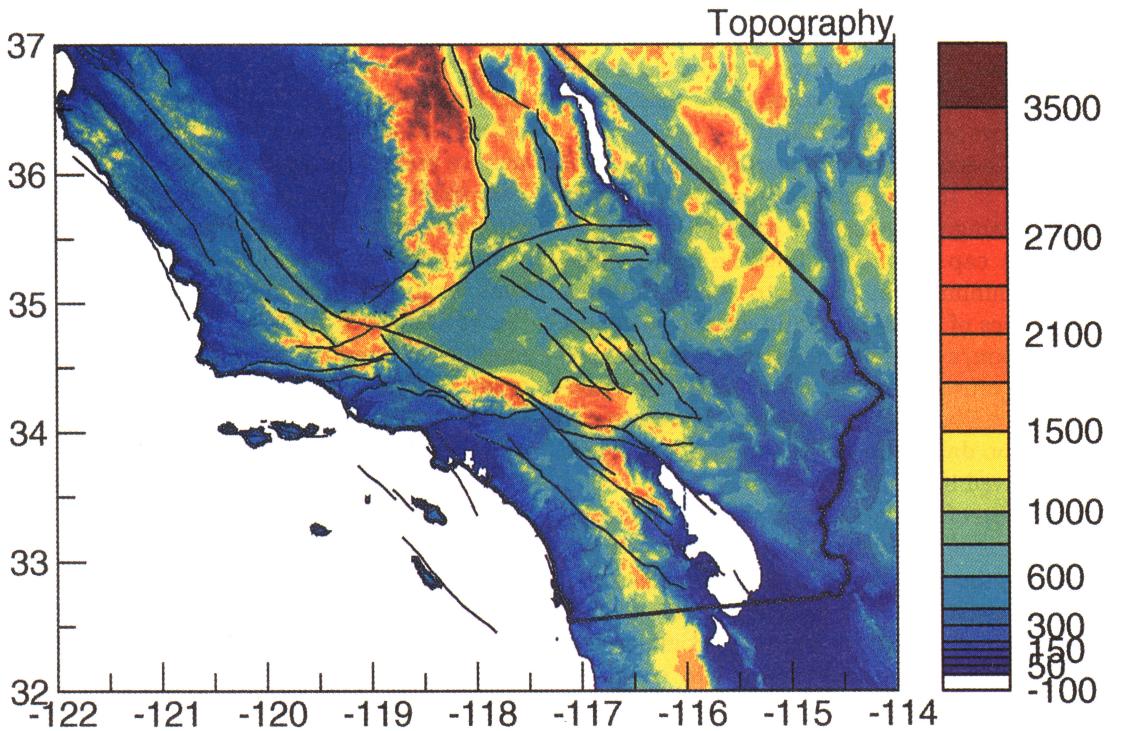

Plate 4. Southern California surface topography in meters. Note that there is a general, but not perfect, correlation of thicker crust with elevated areas and of thinner crust with depressed areas.

Los Angeles Basin, and (5) thicker than average (up to 36 km) crust under the southernmost Sierra Nevada.

Assuming constant crustal and mantle densities (the Airy hypothesis), simple isostatic models require the Moho topography to be a scaled version of the surface topography (by the factor $-\rho_c/(\rho_m - \rho_c)$, where ρ_c and ρ_m are the crust and mantle densities, respectively). This assumes that isostatic balance is the only means of supporting the surface topography and predicts that mountains are underlain by thick crustal roots and Moho depressions. From a comparison of the Moho topography in the top plot of Plate 2 with the surface topography in Plate 4, it seems that at least the sign of the scaling factor agrees with this simple view, with a deeper Moho under elevated areas (e.g., southern Sierra and eastern Transverse Ranges) and a shallow Moho under depressed areas (e.g., Salton Trough and offshore). However, there are also several areas which do not fit this model; for instance, neither the central Transverse Ranges nor the Peninsular Ranges seem to have a crustal root. Other factors influencing topography include lateral density variations in the crust and mantle, elastic strength of the rigid upper crust, and dynamic effects related to mantle flow. Combining our results with gravity studies could help address these issues.

Our crustal thickness results generally agree with those of previous studies. For example, from a series of reflection survey lines in the northwestern Mojave, *Cheadle et al.* [1986] estimate a flat Moho with 33 km of crustal thickness in the northern part of their survey and a flat Moho at 26–29 km depth farther south. *Li et al.* [1992] find a 30 km deep Moho dipping 6° to the south under the north slope of the San Bernardino Mountains, in close agreement with our results. *Malin et al.* [1995] find a flat Moho at 33 km beneath a reflection line in the Tehachapi Mountains, where we find a similar crustal thickness but with a northwest dipping Moho. It is possible that this apparent dip is due to our procedure smoothing out a more sudden change in Moho depth near, but not directly beneath, the Malin et al. profile.

Most of the work done on the crustal structure and thickness of the Sierra Nevada has been concentrated in the High Sierra and farther north (recent examples include *Jones et al.* [1994], *Savage et al.* [1994], and *Wernicke et al.* [1996]). Our coverage ends in the very southernmost Sierra (near the SCSN station ISA); our Moho depth estimate of 36 km in this area agrees well with either of the *Jones et al.* [1994] interpretations of their *Pn* arrival times.

The Salton Trough has anomalously thin crust, as might be expected for an active rift zone. Previous estimates of crustal thickness have ranged from 16 to 19 km [*Hadley,* 1978] (from an unreversed refraction profile) to 25 km [*Sung and Jackson,* 1992] (from *P* travel time tomography). We find Moho depths in this region of 18–19 km, or near the upper end of the *Hadley* [1978]

observations. To test the reliability of our results, we performed our analysis using the local crustal velocity model of *Fuis et al.* [1984] and obtained Moho depths within 1 km of those obtained from the HK model.

The map of our estimates of upper mantle velocity shows high velocities to the northeast and slow velocities to the southwest, with a transition which corresponds closely with the San Andreas Fault. However, recall that our estimates of upper mantle velocity tradeoff directly with our assumed lower crustal velocity, so the most accurate way to interpret these values would be as slowness contrasts across the Moho (relative to our assumed lower crustal slowness of 6.7^{-1} s/km). Our estimates of upper mantle velocity agree well with those from P travel time tomography studies [*Hearn and Clayton,* 1986; *Sung and Jackson,* 1992], except in the Salton Trough and under the southernmost Sierra Nevada.

In the Salton Trough we find upper mantle velocities as low as 7.5 km/s, similar to the results of *Sung and Jackson* [1992], but much lower than the 7.9 to 8.0 km/s of *Hearn and Clayton* [1986]. As described in the synthetic example in the previous section, the very high (up to 7.2 km/s at 16 km depth) lower crustal velocity found by *Fuis et al.* [1984] may be causing our procedure to significantly underestimate the upper mantle velocity, since the Moho velocity contrast is relatively small and we assume 6.7 km/s for the lower crustal velocity. However, this extremely high velocity lower crustal layer will not bias our estimate of crustal thickness significantly since the high-velocity layer is only about 4 km thick.

Most previous studies have found low Pn velocities under the Sierra Nevada [e.g. *Hearn,* 1996; *Sung and Jackson,* 1992; *Jones et al.,* 1994], in disagreement with our velocity estimates of 8.1 to 8.2 km/s for this region. There are several possible explanations for this discrepancy. The first is that we have relatively little data at Pn ranges for our caps in the southern Sierra (note the high noise levels between the Pn and the PmP arrivals and the large scatter in the differential arrival times at ranges beyond 170 km in the southern Sierra stack in Plate 1). Therefore, while the reasonable amount of data at Pg ranges allows us to constrain the crustal thickness, we cannot constrain the upper mantle velocity as well. Another possibility is that there are complications arising from the presence of a several kilometer thick layer with velocities of 7.2 to 7.7 km/s at the top of the mantle underlain by higher (up to 8.1 km/s) velocity material as discussed by *Jones et al.* [1994] and *Savage et al.* [1994]. A third possibility is that our procedure simply does not have the resolution to the detect the relatively narrow area of low Pn velocity under the Sierra and is averaging in the high ($>\sim$8.0 km/s) Pn velocities found both east and west of the Sierra [*Jones et al.* 1994] or that the first arrival picked by our autopicker is an out of plane refraction from these regions of higher mantle velocity.

Areas for future work include combining our results for PmP times with other tomographic studies to remove many of the ambiguities associated with variations in lower crustal velocities. Incorporating $SmS-S$ travel times into our technique could also help remove these ambiguities; unfortunately, so far we have been unable to pick reliable SmS times, even in the stacked data, from these vertical component instruments. Our stacking and modeling techniques appear suitable for other regions with good station coverage and distributed seismicity; for example, extending our analysis to include stations from the northern California and Nevada networks would greatly expand our coverage, particularly for the Sierra Nevada.

Acknowledgments.
We are grateful to the operators and analysts who maintain the USGS/Caltech Southern California Seismic Network and who pick and archive the seismograms and to the personnel at the Southern California Earthquake Center who distribute the data. We thank Jim Mori, Thomas Hearn, and Carl Kisslinger for useful, constructive reviews. This research was supported by USGS/NEHRP grant 1434-94-G-2454.

References

Baker, G. E., J. B. Minster, G. Zandt, and H. Gurrola, Constraints on crustal structure and complex Moho topography beneath Piñon Flat, California, from teleseismic receiver functions, *Bull. Seismol. Soc. Am., 86,* 1830-1844, 1996.

Cheadle, M. J., B. L. Czuchra, T. Byrne, C. J. Ando, J. E. Oliver, L. D. Brown, S. Kaufman, P. E. Malin, and R. A. Phinney, The deep crustal structure of the Mojave Desert, California, from COCORP seismic reflection data, *Tectonics, 5,* 293-320, 1986.

Earle, P. S., and P. M. Shearer, Characterization of global seismograms using an automatic-picking algorithm, *Bull. Seismol. Soc. Am., 84,* 366-376, 1994.

Fuis, G. S., W. D. Mooney, J. H. Healy, G. A. McMechan, and W. J. Lutter, A seismic refraction survey of the Imperial Valley Region, California, *J. Geophys. Res., 89,* 1165-1189, 1984.

Hadley, D., Geophysical investigations of the structure and tectonics of southern California, Ph.D. thesis, Calif. Inst. of Technol., Pasadena, 1978.

Hadley, D., and H. Kanamori, Seismic structure of the Transverse Ranges, California, *Geol. Soc. Am. Bull., 88,* 1469-1478, 1977.

Hearn, T. M., Pn travel times in southern California, *J. Geophys. Res., 89,* 1843-1855, 1984.

Hearn, T. M., Anisotropic Pn tomography in the western United States, *J. Geophys. Res., 101,* 8403-8414, 1996.

Hearn, T. M., and R. W. Clayton, Lateral velocity variations in southern California, II, Results for the lower crust from Pn waves, *Bull. Seismol. Soc. Am., 76,* 511-520, 1986.

Jones, C. H., H. Kanamori, and S. W. Roecker, Missing roots and mantle "drips": Regional P_n and teleseismic arrival times in the southern Sierra Nevada and vicinity, California, *J. Geophys. Res., 99,* 4567-4601, 1994.

Kanamori, H., and D. Hadley, Crustal structure and temporal velocity change in southern California, *Pure Appl. Geophys., 113,* 257-280, 1975.

Kanasewich, E.R., *Time Series Analysis in Geophysics*, Univ. of Alberta Press, Edmonton, 1973.

Li, Y.-G., T. L. Henyey, and P. C. Leary, Seismic reflection constraints on the structure of the crust beneath the San Bernardino Mountains, Transverse Ranges, southern California, *J. Geophys. Res., 97,* 8817-8830, 1992.

Magistrale, H., H. Kanamori, and C. Jones, Forward and inverse three-dimensional *P* wave velocity models of the southern California crust, *J. Geophys. Res., 97,* 14,115-14,135, 1992.

Malin, P. E., E. D. Goodman, T. L. Henyey, Y.-G. Li, D. A. Okaya, and J. B. Saleeby, Significance of seismic reflections beneath a tilted exposure of deep continental crust, Tehachapi Mountains, California, *J. Geophys. Res., 100,* 2069-2087, 1995.

Mori, J., and D. Helmberger, Large-amplitude Moho reflections (*SmS*) from Landers aftershocks, southern California, *Bull. Seismol. Soc. Am., 86,* 1845-1852, 1996.

Prodehl, C., Seismic refraction study of crustal structure in the western United States, *Geol. Soc. Am. Bull., 81,* 2629-2646, 1970.

Savage, M. K., L. Li, J. P. Eaton, C. H. Jones, and J. N. Brune, Earthquake refraction profiles of the root of the Sierra Nevada, *Tectonics, 13,* 803-817, 1994.

Somerville, P., and J. Yoshimura, The influence of critical Moho reflections on strong ground motions recorded in San Francisco and Oakland during the 1989 Loma Prieta earthquake, *Geophys. Res. Lett., 17,* 1203-1206, 1990.

Sung, L.-Y., and D. D. Jackson, Crustal and uppermost mantle structure under southern California, *Bull. Seismol. Soc. Am., 82,* 934-961, 1992.

Vetter, U., and J. B. Minster, P_n velocity anisotropy in southern California, *Bull. Seismol. Soc. Am., 71,* 1511-1530, 1981.

Wald, L. A., L. K. Hutton, and D. D. Given, The Southern California Network Bulletin: 1990-1993 summary, *Seismol. Res. Lett., 66,* 9-19, 1995.

Wernicke, B., et al., Origin of high mountains in the continents: The southern Sierra Nevada, *Science, 271,* 190-193, 1996.

Zhao, D., and H. Kanamori, Simultaneous inversion of local and teleseismic data for the crust and mantle structure of southern California, *Phys. Earth Planet. Inter., 93,* 191-214, 1996.

Zhu, L., and H. Kanamori, Variation of crustal thicknesses in southern California from teleseismic receiver functions at TERRAscope stations, *Eos Trans. AGU, 75* (44), Fall Meet. Suppl., 484, 1994.

K. B. Richards-Dinger and P. M. Shearer, Institute of Geophysics and Planetary Physics, Scripps Institution of Oceanography, University of California, San Diego, La Jolla, CA 92093-0225. (e-mail: kdinger@ucsd.edu)

(Received June 10, 1996; revised January 30, 1997; accepted March 17, 1997.)